HNUE JOURNAL OF SCIENCE
Natural Sciences 2025, Volume 70, Issue 3, pp. 74-82
This paper is available online at http://hnuejs.edu.vn/ns
DOI: 10.18173/2354-1059.2025-0038

OPTIMAL PARTICLE SIZE OF Ag_3PO_4 PHOTOCATALYSTS ACHIEVED BY pH-CONTROLLED SYNTHESIS

Pham Do Chung[1,*], Lam Thi Hang[2], La Thi Bich Dao[1] and Le Thi Mai Oanh[1]

[1]*Faculty of Physics, Hanoi National University of Education, Hanoi city, Vietnam*

[2]*Faculty of Natural Sciences, Electric Power University, Hanoi city, Vietnam*

*Corresponding author: Pham Do Chung, e-mail: chungpd@hnue.edu.vn

Received August 26, 2025. Revised September 9, 2025. Accepted September 30, 2025.

Abstract. Silver orthophosphate (Ag_3PO_4, APO) was synthesized by a simple co-precipitation method using $AgNO_3$ and $K_2HPO_4.3H_2O$ as precursors. The pH of the precursor solution was adjusted by adding a HNO_3 solution (0.5 M), which effectively controlled the particle size without altering the crystal structure. The samples in this work were prepared as APO–xH, where x represents the volume (mL) of HNO_3 added (0, 0.5, 1.0, 1.5, 2.0, and 2.5 mL). The particle size decreased systematically from ~450 nm (APO–0H) to ~150 nm (APO–2.5H). APO–1.5H, with an average size of ~250 nm, represented the "optimal size," achieving complete degradation of 10 ppm Rhodamine B within 14 minutes under visible light irradiation from a 50 W compact fluorescent lamp, twice as fast as pristine APO. In preliminary cycling performed only on the reference APO–0H sample, the RhB degradation efficiency decreased to ~30% by the fifth cycle under visible-light irradiation. These findings confirm that the optimal photocatalytic activity of Ag_3PO_4 does not originate solely from increased surface area but from a balance between particle size, morphology, and structural stability. This work provides a simple approach to tailor Ag_3PO_4 for efficient visible-light-driven water treatment.

Keywords: photocatalytic, silver phosphate, particle size.

1. Introduction

Silver orthophosphate (Ag_3PO_4, APO) is a much better photocatalytic material than some basic photocatalysts such as TiO_2 and ZnO. Because APO has an optical band gap of 2.36 - 2.45 eV (absorption edge ≈ 506 - 525 nm), it absorbs UV and part of the visible

spectrum, enabling photocatalysis under solar/visible illumination [1]-[3]. It is capable of decomposing a wide range of organic pollutants, including rhodamine B, bisphenol A, phenol, methylene blue, quinoline yellow, and methyl orange [4]-[6]. Despite these advantages, its practical use is limited by short catalyst lifetime and self-degradation during operation [2], [7], [8].

To address this problem, some of our previous works have focused on preparing Ag/Ag_3PO_4 composites to enhance stability, constructing $Ag_3PO_4/g\text{-}C_3N_4$ heterostructures, and tuning the Ag^+/PO_4^{3-} ratio or phosphate source to adjust crystallinity and morphology, all aimed at improving the stability of the APO photocatalyst. Following these results, we observed that the photocatalytic performance of Ag_3PO_4 is strongly influenced by morphology and particle size, which depend on synthesis parameters such as the precursor salt, pH, and the presence of surfactants [2], [5], [7]. For example, Na_2HPO_4 derived samples with pseudo-spherical morphology exhibited higher activity in methylene blue degradation, while synthesis using phosphoric acid produced tetrahedral particles [9], [10]. Decreasing pH via ammonia addition also yielded smaller particles with higher activity [5]. Extremely small nanoparticles (~10 nm) showed very high photocatalytic efficiency but poor stability after several cycles [7]. These results confirm that precursor chemistry and pH play a decisive role in tailoring particle size and performance [2], [5], [7].

Therefore, in this study, we attempted to synthesize APO from $AgNO_3/K_2HPO_4$ and control its particle size by adjusting the pH through the addition of a 0.5 M HNO_3 solution. This work aimed to find an "optimal particle size" of APO that maximizes photocatalytic activity while maintaining acceptable stability. Unlike previous reports that mainly described size effects qualitatively, this work systematically correlates photocatalytic rate constants with particle size and identifies ~250 nm as the optimal regime where activity and stability are balanced.

2. Content

2.1. Materials and methods

Ag_3PO_4 samples were synthesized from two precursors, silver nitrate ($AgNO_3$, 99%) and dipotassium hydrogen phosphate trihydrate ($K_2HPO_4 \cdot 3H_2O$, 99%), by a co-precipitation method. Briefly, $AgNO_3$ and $K_2HPO_4 \cdot 3H_2O$ were dissolved separately in distilled water to form 0.02 M solutions. To control the precursor pH, different volumes of 0.5 M HNO_3 were added to the phosphate solution before mixing. The acidified phosphate solution was then added dropwise into the silver nitrate solution under constant stirring, and the mixture was stirred for 3 h at room temperature. The resulting precipitate was filtered, washed with distilled water, and dried at 100 °C to obtain Ag_3PO_4 powder. The samples were denoted as APO–0H, APO–0.5H, APO–1.0H, APO–1.5H, APO–2.0H, and APO–2.5H, where the number indicates the volume (mL) of HNO_3 added to the precursor solution.

The crystalline phase was analyzed by X-ray diffraction (XRD, Bruker D8 Advance, Cu Kα radiation, λ = 1.54064 Å). The morphology was examined by scanning electron microscopy (SEM, Hitachi S-4800). Optical properties were investigated using UV-vis diffuse reflectance spectroscopy (Jasco V770). Specific surface areas were determined by N_2 adsorption-desorption measurements at 77 K on a Micromeritics TriStar 3000

analyzer, and BET surface areas were calculated from the adsorption data in the relative pressure range of 0.05-0.30.

Photocatalytic activity was evaluated under visible light using 50 W compact fluorescent lamps as the irradiation source. For each test, 0.06 g of Ag_3PO_4 was dispersed in 30 mL of distilled water and stirred for 30 min. Then, 30 mL of 20 ppm dye solution (RhB) was added, giving a final concentration of 10 ppm. The suspension was stirred in the dark for 30 min to reach adsorption-desorption equilibrium, with aliquots taken for analysis. Afterward, the suspension was irradiated with visible light, and aliquots were collected at regular intervals, centrifuged to remove the photocatalyst, and analyzed by UV-vis spectroscopy at characteristic wavelengths (554 nm).

2.2. Results and discussion

The crystal structures of the synthesized Ag_3PO_4 samples were characterized by X-ray diffraction (XRD), as shown in Figure 1. All diffraction peaks (13 peaks in the range 2θ = 20-80°) match well with the standard cubic Ag_3PO_4 phase (JCPDS No. 06-0505), indexed to the characteristic (110), (200), (210), (211), (310), (320), and related reflections. The XRD patterns display sharp and symmetric peaks, indicating high crystallinity. No additional peaks were observed, confirming that all samples are phase-pure without detectable impurities. The refined lattice parameter derived from the (210) reflection a ≈ 6.0 Å, consistent with reported values for the body-centered cubic (BCC, space group $P4_3n$) Ag_3PO_4 structure [2], [5].

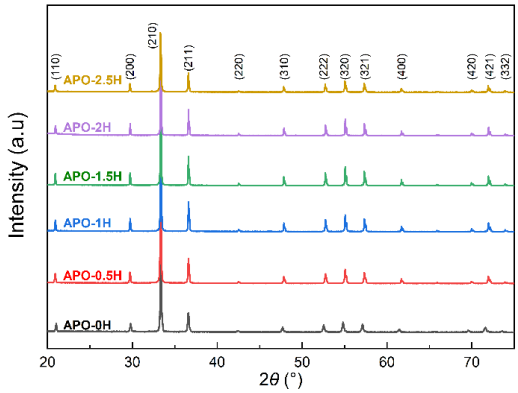

Figure 1. XRD patterns of Ag_3PO_4 samples synthesized with different volumes of HNO_3 (0.5 M): APO-0H, APO-0.5H, APO-1.0H, APO-1.5H, APO-2.0H, and APO-2.5H

According to previous calculations and simulations, the BCC phase is the thermodynamically stable structure of Ag_3PO_4, and is therefore consistently obtained by simple co-precipitation routes [7]-[9]. Our previous reports have shown that variations in precursor chemistry (e.g., monobasic vs. dibasic phosphate salts) or synthesis conditions (e.g., addition rate of solutions, local pH) mainly affect particle size and morphology rather than inducing a phase transition [8], [9]. In this work, all samples maintained the stable BCC phase, and the key difference arose only from size control by adjusting the precursor pH with HNO_3 (0.5M).

The vibrational characteristics of the synthesized samples were investigated by Raman spectroscopy (Figure 2). All spectra exhibit a strong band at ~909 cm^{-1}, assigned

to the symmetric stretching mode of PO_4^{3-} tetrahedra [10]. The peak observed at ~406 cm^{-1} is attributed to the symmetric bending of P-O-P bonds. These features are consistent with previously reported spectra of crystalline Ag_3PO_4 and confirm the formation of the expected phosphate framework.

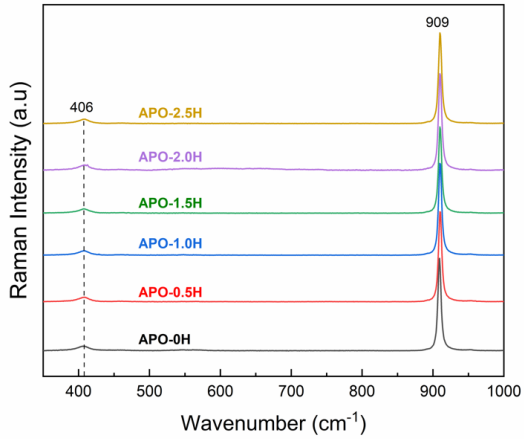

Figure 2. Raman spectra of Ag_3PO_4 synthesized with different volumes of HNO_3 (0.5 M): APO-0H, APO-0.5H, APO-1.0H, APO-1.5H, APO-2.0H, and APO-2.5H

The Raman profiles of all samples remain essentially unchanged with increasing HNO3 content in the precursor solution, indicating that pH adjustment affects particle size but does not alter the local structure of PO_4^{3-} units or the overall crystal symmetry. This observation, in agreement with the XRD results, demonstrates that the co-precipitation method yields phase-pure Ag_3PO_4 with stable lattice vibrations regardless of synthesis conditions.

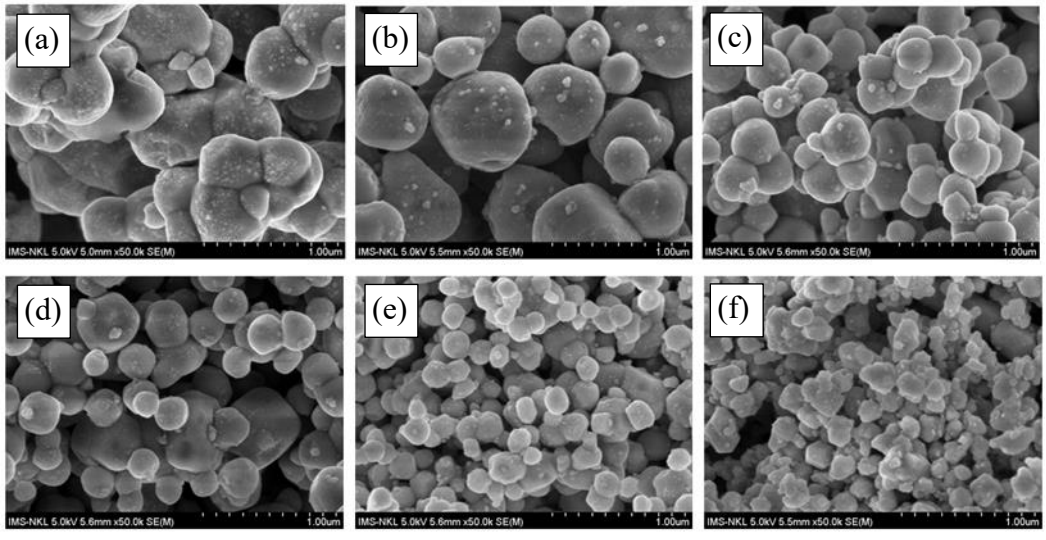

Figure 3. SEM images of Ag_3PO_4 samples synthesized with different volumes of HNO_3 (0.5 M): APO-0H (a), APO-0.5H (b), APO-1.0H (c), APO-1.5H (d), APO-2.0H (e), and APO-2.5H (f)

SEM images of all samples (Figure 3) reveal a pseudo-spherical particle morphology, typical of Ag_3PO_4 obtained by co-precipitation. The APO–0H sample (without HNO_3)

shows large particles with diameters of 300-600 nm, often aggregated into clusters of several grains. The particle size progressively decreases as the volume of HNO_3 increases. For APO–1.5H, the average particle size is ~250 nm with a relatively uniform distribution; the particles are well dispersed with clear grain boundaries. In contrast, further increasing HNO_3 yields smaller particles (~150 nm for APO–2.5H), but these exhibit stronger agglomeration with fused particles and indistinct boundaries.

The SEM results show that the precursor pH plays a crucial role in determining the morphology and particle size of Ag_3PO_4. Importantly, while reducing particle size increases surface area, excessive reduction tends to promote aggregation, which can limit the effective surface available for photocatalysis. Two opposing processes - particle size reduction and particle agglomeration - directly affect the photocatalytic performance. Therefore, it is necessary to identify an optimal condition where Ag_3PO_4 exhibits both high activity and improved long-term stability.

To quantify the particle size, image analysis was performed on the SEM images of the Ag_3PO_4 samples. Figure 4 illustrates the particle size distribution for APO–0H, APO–0.5H, APO–1.0H, APO–1.5H, APO–2.0H, and APO–2.5H. The results reveal a monotonic decrease in mean particle diameter from ~450 nm (APO–0H) to ~150 nm (APO–2.5H). However, the size distribution becomes narrower and more uniform at ~250 nm for APO–1.5H, whereas APO–2.5H shows a broader distribution due to agglomeration. These results from XRD, Raman, and SEM demonstrate that precursor pH effectively controls particle size and surface morphology but does not induce any phase transition or alter the phosphate bonding framework, thereby preserving the intrinsic stability of the BCC Ag_3PO_4 lattice.

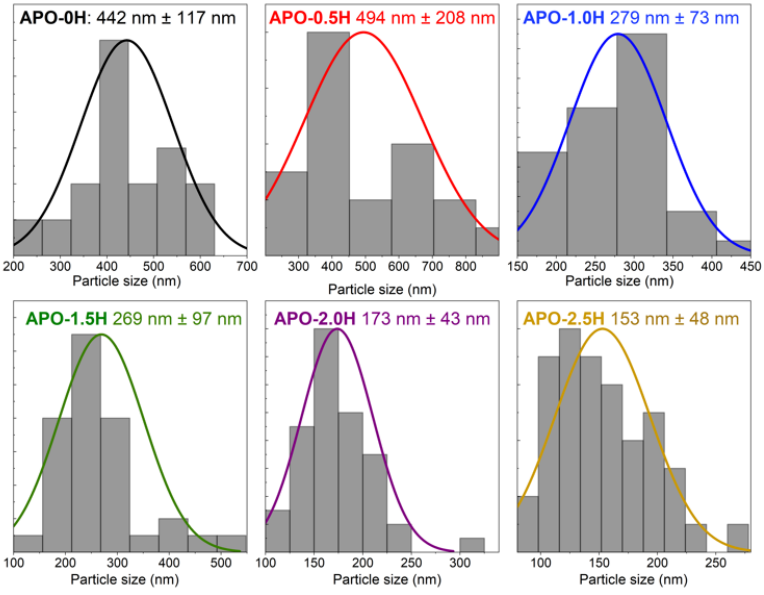

Figure 4. Particle size distributions of Ag_3PO_4 samples synthesized with different volumes of HNO_3 (0.5 M): APO-0H, APO-0.5H, APO-1.0H, APO-1.5H, APO-2.0H, and APO-2.5H

The N_2 adsorption-desorption isotherms (Figure 5a) show that APO–2.5H exhibits a slightly higher adsorption capacity than APO–1.5H, which is consistent with the BET

surface areas of 0.98 and 0.82 m²/g, respectively. The BET plots (Figure 5b) confirm good linearity, indicating reliable surface area determination.

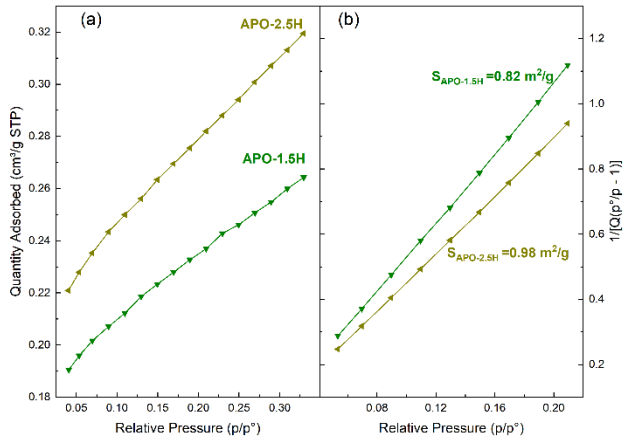

Figure 5. The N_2 adsorption–desorption isotherms (a) and the BET fit (b) of APO-1.5H and APO-2.5H

Figure 6 presents the UV-vis absorption spectra of Ag_3PO_4 samples synthesized with different volumes of 0.5 M HNO_3, together with the corresponding band-gap determination from Tauc plots. All APO samples exhibited strong absorption in the visible region with an absorption edge at ~520 nm (Figure 6a). The optical band gap, estimated from Tauc plots assuming a direct-allowed transition (n = 1/2), is ~2.41 eV for all samples and is consistent with reported values of 2.36-2.45 eV for Ag_3PO_4 [2], [5], [9]. These results confirm the reliability of the synthesis and indicate that pH adjustment, while reducing particle size with increasing HNO_3 content, does not alter the intrinsic electronic structure of Ag_3PO_4.

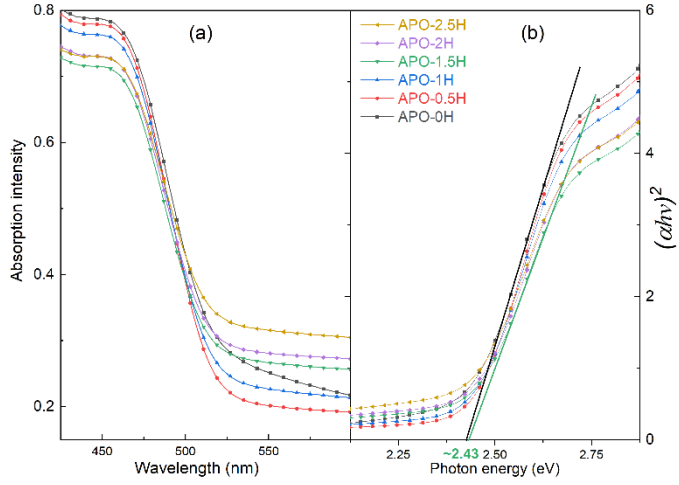

Figure 6.* UV–*vis absorption spectra (a) and corresponding Tauc plots (b) of Ag_3PO_4 samples synthesized with different volumes of HNO_3 (0.5 M): APO-0H, APO-0.5H, APO-1.0H, APO-1.5H, APO-2.0H, and APO-2.5H

The photocatalytic activities of Ag_3PO_4 samples with different particle sizes were evaluated by degrading 10 ppm RhB under a 50 W compact fluorescent lamp (Figure 7).

The lamp delivered a luminous flux of ~3150 lm at the solution surface, corresponding to an average irradiance of ~250 $W.m^{-2}$, which is roughly one-quarter of the standard solar intensity (1 SUN, ~1000 $W.m^{-2}$). All samples showed negligible dark adsorption (≤10%), while rapid degradation occurred under visible light. APO–0H completed RhB removal within ~30 min, whereas smaller-sized samples degraded faster. APO–1.5H exhibited the highest activity, achieving complete degradation in ~14 min.

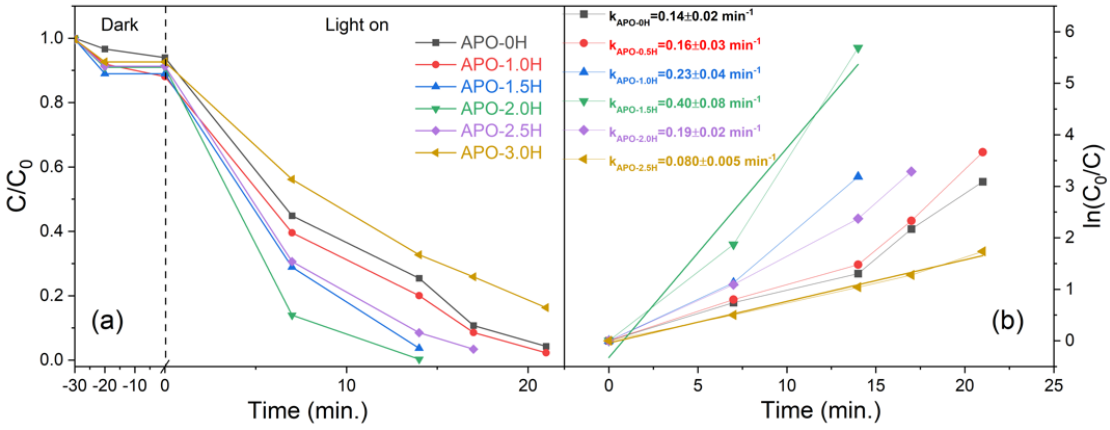

Figure 7. Photocatalytic degradation of RhB (10 ppm) by Ag_3PO_4: comparison of C/C_0 vs. time (a) and corresponding pseudo-first-order fits $ln(C_0/C)$ (b) for APO-0H, APO-0.5H, APO-1.0H, APO-1.5H, APO-2.0H, and APO-2.5H

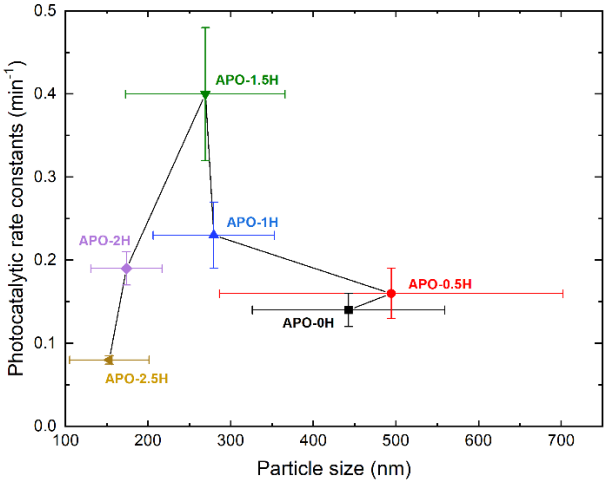

Figure 8. Photocatalytic rate constants (k) of Ag_3PO_4 samples plotted against mean particle size, highlighting the optimum at ~250 nm (APO-1.5H)

The photocatalytic kinetics of all APO samples were fitted using a pseudo-first-order model ($ln(C_0/C) = kt$), and the resulting rate constants ranged from 0.080 ± 0.005 min^{-1} to 0.40 ± 0.08 min^{-1} (as summarized in Figure 7). As size decreased from ~450 nm (APO–0H) to ~250 nm (APO–1.5H), k increased steadily; further downsizing to ~150 nm (APO–2.5H) reduced k, evidencing a non-monotonic size dependence with a clear maximum at ~250 nm. This trend reflects the competition between enhanced surface reactivity at smaller sizes and the adverse effects of agglomeration/instability at very fine sizes. To better visualize this relationship, Figure 8 plots k as a function of particle size.

Although APO–2.5H shows a larger BET surface area (0.98 m^2/g) than APO–1.5H (0.82 m^2/g), its activity is lower, indicating that surface area alone does not dictate performance. Together with the nearly identical band gap (~2.41 eV) across samples, these results confirm that particle size and associated surface characteristics, rather than electronic structure, govern the observed activity.

The stability of Ag_3PO_4 was evaluated by repeated photocatalytic degradation of RhB under visible light (Figure 9). The degradation efficiency decreased to ~30% after the fifth cycle, consistent with the well-known limited durability of Ag_3PO_4, generally attributed to photocorrosion and the reduction of Ag^+ to metallic Ag during operation. Reusability tests were not performed for all size variants; thus, a systematic stability comparison (particularly for APO–1.5H and APO–2.5H) is outside the scope of the present study.

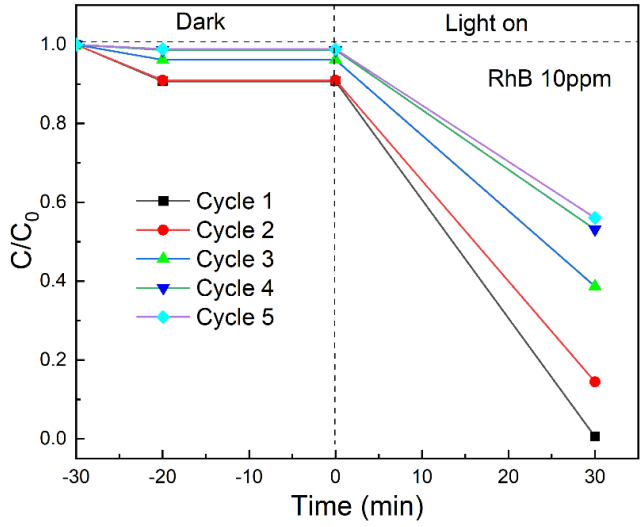

Figure 9. Degradation efficiency of APO-0H over five consecutive photocatalytic cycles (RhB, visible light)

3. Conclusions

This study demonstrates that precursor-pH control enables tuning of Ag_3PO_4 particle size without altering its crystal phase or band gap. Photocatalytic kinetics reveal dependence on both particle size and surface morphology, with the best performance observed for APO–1.5H (~250 nm), where uniformly distributed and well-dispersed particles completely degraded RhB in 14 min under visible light, giving rate constants of 0.40 ± 0.08 min^{-1}. Beyond confirming size as a critical parameter, these findings highlight the limitation of excessive downsizing: ~150 nm particles suffer from aggregation and photocorrosion, leading to poor reusability. It should be noted, however, that reusability was tested only for APO–0H, which remains a limitation of this study.

Acknowledgment. This study was funded by the Ministry of Education and Training, Vietnam, under grant number B2024-SPH-08.

REFERENCES

[1] Huang GF, Ma ZL, Huang WQ, Tian Y, Jiao C, Yang ZM, Wan Z, Pan A, (2013). Ag_3PO_4 Semiconductor Photocatalyst: Possibilities and Challenges. *Journal of Nanomaterials*, 371356. DOI: 10.1155/2013/371356.

[2] Chen D, Cheng Y, Zhou N, Chen P, Wang Y, Li K, Huo S, Cheng P, Peng P, Zhang R, Wang L, Liu H, Liu Y, Ruan R, (2020). Photocatalytic degradation of organic pollutants using TiO_2-based photocatalysts: A review. *Journal of Cleaner Production*, 268, 121725. DOI: 10.1016/J.JCLEPRO.2020.121725.

[3] Nguyen MH, Le TMO, Pham DC, Dao VT, Vu TM, Lam TH, Nguyen VM, (2023). Tuning the particle size, physical properties, and photocatalytic activity of Ag_3PO_4 materials by changing the $Ag^+/(PO_4)^{3-}$ ratio. *Chinese Physics B*, 32, 038102. DOI: 10.1088/1674-1056/AC84CE.

[4] He G, Yang W, Zheng W, Gong L, Wang X, An Y, Tian M, (2019). Facile controlled synthesis of Ag_3PO_4 with various morphologies for enhanced photocatalytic oxygen evolution from water splitting. *RSC Advance,* 9, 18222. DOI: 10.1039/C9RA01306G.

[5] Amornpitoksuk P, Intarasuwan K, Suwanboon S, Baltrusaitis J, (2013). Effect of phosphate salts (Na_3PO_4, Na_2HPO_4, and NaH_2PO_4) on Ag_3PO_4 morphology for photocatalytic dye degradation under visible light and toxicity of the degraded dye products. *Industrial & Engineering Chemistry Research*, 52(49), 17369-17375. DOI: 10.1021/ie401821w.

[6] Yu C, Chen X, Li N, Zhang Y, Li S, Chen J, Yao L, Lin K, Lai Y, Deng X, (2022). Ag_3PO_4-based photocatalysts and their application in organic-polluted wastewater treatment. *Environmental Science and Pollution Research*, 29, 18423-18439. DOI: 10.1007/S11356-022-18591-7.

[7] Wang JD, Wang FR, Liu JK, Yang XH, Zhong XH, (2016). Controlled synthesis and characterization of thermo-stabilized Ag_3PO_4 crystals. *Research on Chemical Intermediates,* 42, 8285-8304. DOI: 10.1007/s11164-016-2596-6.

[8] Zheng W, Yang W, He G, Chi J, Duan Y, Chen M, Liu M, (2019). Facile synthesis of extremely small Ag_3PO_4 nanoparticles on hierarchical hollow silica sphere (HHSS) for the enhanced visible-light photocatalytic property and stability. *Colloids and Surfaces A*, 571, 1-8. DOI: 10.1016/j.colsurfa.2019.03.044.

[9] Nguyen MH, Le TMO, Pham DC, Vu TM, Nguyen TDA, La TBD, Lam TH, Pham TD, Nguyen VM, (2022). Effect of monobasic/dibasic phosphate salts on the crystallinity, physical properties, and photocatalytic performance of Ag_3PO_4 material. *AIMS Materials Science*, 5, 770-784. DOI: 10.3934/MATERSCI.2022047.

[10] Botelho G, Sczancoski JC, Andres J, Gracia L, Longo E, (2015). Experimental and Theoretical Study on the Structure, Optical Properties, and Growth of Metallic Silver Nanostructures in Ag_3PO_4. *The Journal of Physical Chemistry C*, 119(11), 6293-6306. DOI: 10.1021/jp512111v.